Journal of Power Sources 199 (2012) 247–255

Contents lists available at SciVerse ScienceDirect

Journal of Power Sources

journal homepage: www.elsevier.com/locate/jpowsour

Bipolar plate cell design for a lithium air battery

Jim Adams*, Mohan Karulkar[1]

Ford Motor Company, 2101 Village Road, MD 3179, Dearborn, MI 48124, USA

ARTICLE INFO

Article history:
Received 23 September 2011
Accepted 12 October 2011
Available online 17 October 2011

Keywords:
Automotive
Bipolar
Plate
Lithium
Air
Battery

ABSTRACT

The performance and cost of a bipolar plate cell design for a 40 kWh lithium-air battery was estimated and compared to USABC goals. A bipolar plate cell design for a lithium-air battery can meet the cell performance goals, provided certain cell design targets are met. In particular, the excess lithium should be <2×, the current density should be >40 mA cm^{-2}, the cathode capacity should be >1650 mAh g^{-1} carbon, and the bipolar plate material density should be <5 g cm^{-3}. Meeting the above targets, the specific and volumetric energy densities for the lithium-air cell were estimated at 640 Wh kg^{-1} and 600 Wh l^{-1}, respectively; the specific and volumetric power densities were estimated at 1310 W kg^{-1} and 1220 W l^{-1}, respectively. However, the system cost goal of \$100 kWh^{-1} for electric vehicles was not met; the cost of a 40 kWh lithium-air battery system using a bipolar plate design was estimated at \$238 kWh^{-1}.

1. Introduction

Substantial improvement in the performance of rechargeable batteries is required for widespread commercialization of electric vehicles. State-of-the-art (SOA) lithium-ion technology using graphitic carbon and inorganic oxides delivers ~180 Wh kg^{-1}, and a two-fold improvement based on new materials using similar chemistry [1] is likely the most that can be expected. Lithium-air batteries present an attractive alternative, harnessing the energy created by the reaction of a lithium metal anode and an oxygen-accessible porous cathode [1–8]. Although the theoretical specific energy density of a lithium–oxygen couple of 12 kWh kg^{-1} greatly exceeds the United States Advance Battery Consortium (USABC) long term goal for an electric vehicle (EV) of 400 Wh kg^{-1} by a factor of 30×, it remains a challenge to design a lithium-air cell that simultaneously meets the energy density, power density, and system cost targets necessary for application in an EV.

In spite of the recent increase in research on lithium-air batteries in the areas of cathode capacity, catalysis, influence of electrolyte composition, etc., limited research has been done on estimating the performance of practical lithium-air cells or systems. Zheng et al. [9] developed a model to investigate realizable lithium-air cathode capacity, and demonstrated the importance of cathode porosity and electrode/electrolyte weight on the departure from theoretical capacity. Wagner et al. [10] recognized the need for air distribution mechanisms and lithium safety considerations, and the effect these systems would have on practical energy and power density in a vehicle.

Three specific technical challenges remain to be solved before lithium-air batteries can be considered for commercial automotive applications: (1) the lab-scale cell designs used for lithium-air research are not suitable for automotive applications; (2) SOA lithium-air cells achieve low current densities, and thus low power densities, even when operating on pure oxygen; and (3) the cycle life of SOA lithium-air cells is at least two orders of magnitude below commercialization requirements.

In addition, an automotive cell design must satisfy three criteria: (1) be amenable to high-volume/low-cost manufacturing and assembly; (2) minimize mass and volume while maximizing energy and power densities; and (3) operate efficiently on air. The third criterion of operating on air is probably the most challenging for lithium-air automotive applications, yet PEM fuel cell experience has shown that air is the only technically viable option for an oxidant source in vehicles. Pure oxygen is difficult to store efficiently onboard the vehicle and complicates refueling, while onboard purification of oxygen from air requires excessive amounts of parasitic power.

The two most commonly used lab-scale research cell designs, pouch cells [2–5] and Swagelok® cells [11–13], do not satisfy any of the automotive design criteria. Given the design criteria for a lithium-air cell highlighted above, a PEM fuel cell bipolar plate design is a logical starting point for a lithium-air cell. Besides satisfying the criteria above, a bipolar plate cell design can yield higher current densities due to a more uniform current distribution and better utilization of active materials. In addition, the scalability of the bipolar plate cell design allows for a natural progression from

* Corresponding author. Tel.: +1 313 594 0832; fax: +1 313 621 0646.
E-mail addresses: jadams23@ford.com (J. Adams), mkarulka@ford.com (M. Karulkar).
[1] Tel.: +1 313 248 5699.

0378-7753/$ – see front matter © 2011 Elsevier B.V. All rights reserved.
doi:10.1016/j.jpowsour.2011.10.041

Table 1
Input parameters.

Name	Symbol	Units	Typical value	Design target
Pack energy	E_{pack}	kWh	40	40
Cell current density	i	mA cm^{-2}	42	>40
Cathode capacity	C_{cath}	mAh g^{-1} carbon	1650	≥1650
Density of plate material	ρ_{plate}	g cm^{-3}	2.7	<5.0
Excess lithium	Li_{ex}	Dimensionless	2.0	<2.0
Excess pore volume	$V_{ex\ pore}$	Dimensionless	1.3	≤1.3
Plate active area	A_{plate}	cm^2	500	≤800
Anode thickness	z_{anode}	μm	200	≤200
Separator thickness	z_{sep}	μm	25	–
Flow field depth	$z_{flow\ field}$	μm	200	≤200
Unstamped plate thickness	$z_{unst\ plate}$	μm	200	–
% Carbon in cathode	x	%	60	–
% Li_2O_2 in discharge product		%	100	–
Number of cells	N_{cells}	Dimensionless	1434	–

research to full-size cells and from single cell to multi-cell stack testing.

While the bipolar plate cell design possesses significant advantages over lab-scale research cell designs, it also incurs penalties from the volume and mass necessary to introduce air into the cell, which affect the energy and power densities. In this study, the suitability of a lithium-air bipolar plate cell design for automotive applications was evaluated, and cell design parameters, such as current density, necessary to meet performance targets were determined. The targets for this study were based on the long-term battery goals from the USABC for widespread deployment of EVs [14]. To develop cell target values, a 50% mass and volume packing fraction was assumed in this study. For example, the system-level specific energy density target of 200 Wh kg^{-1} corresponds to a cell specific energy density target of 400 Wh kg^{-1}. A design tool estimated the mass and volume of the bipolar plate cell components and calculated the energy and power densities for lithium-air cells. In addition, a lithium-air system cost was estimated based on a high volume PEM fuel cell system cost estimate. The results established values for cell design parameters that achieve the performance targets and identified areas requiring further research.

2. Design tool description

A schematic of an experimental bipolar plate cell for a lithium-air battery cell is shown in Fig. 1. The cell consists of the cathode flow field/current collector, free-standing cathode, separator, lithium metal anode, and anode current collector. Multiple assemblies can be combined to form a multi-cell stack. The design tool outlined below generates estimates for specific and volumetric energy and power densities for the cell, given the input parameters in Table 1, which shows typical values used in the design tool, and also the cell design targets generated during the study. Constants are listed in Table 2.

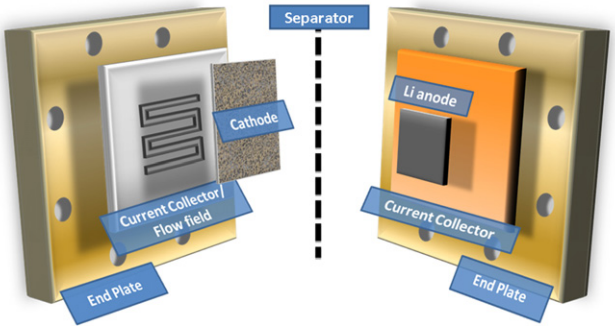

Fig. 1. Bipolar plate flow cell for lithium air batteries.

The theoretical or minimum mass of lithium in the battery pack ($M_{Li\ th}$) is based on the battery pack energy for the vehicle

$$M_{Li\ th} = \frac{E_{pack} \times MW_{Li}}{CV_{disch} \times F \times n} \times 1000 \times 3600 \quad (1)$$

where E_{pack} is the pack energy, MW_{Li} is the atomic weight of lithium, CV_{disch} is the cell discharge voltage, F is Faraday's constant, n is the number of equivalents per g-mol, and 1000 and 3600 are unit conversions from kW to W and h to s, respectively. In this study, the pack energy was held constant at 40 kWh.

In a practical battery, the total mass of lithium in the pack ($M_{Li\ tot}$) must be larger than the theoretical mass to account for capacity fade, etc.

$$M_{Li\ tot} = M_{Li\ th} \times Li_{ex} \quad (2)$$

where Li_{ex} is the excess lithium multiplier, with values ≥1.

The total volume ($V_{Li\ tot}$) and surface area ($A_{Li\ tot}$) of lithium in the pack are

$$V_{Li\ tot} = \frac{M_{Li\ tot}}{\rho_{Li}} \quad (3)$$

$$A_{Li\ tot} = \frac{V_{Li\ tot}}{z_{anode}} \times 10,000 \quad (4)$$

where ρ_{Li} is the density of lithium, z_{anode} is the anode thickness, and 10,000 is the unit conversion from microns to cm.

The number of cells in the pack (N_{cells}) is equal to

$$N_{cells} = \frac{A_{Li\ tot}}{A_{plate}} \quad (5)$$

where A_{plate} is the active area of the cell. A_{plate} does not include extra area necessary for inlet and outlet manifolds, seals, etc, which can be as high as 20% of the active area.

Table 2
Constants.

Name	Symbol	Units	Value
Cell discharge voltage	CV_{disch}	V	2.7
Faraday's constant	F	C equiv.$^{-1}$	96,500
Number of equivalents	n	equiv. g^{-1} mol	1
MW Li	MW_{Li}	g gmol^{-1}	6.94
MW Li_2O_2	$MW_{Li_2O_2}$	g gmol^{-1}	45.88
Density of lithium	ρ_{Li}	g cm^{-3}	0.535
Density of separator	ρ_{sep}	g cm^{-3}	0.610
Density Li_2O_2	$\rho_{Li_2O_2}$	g cm^{-3}	1.206
Density carbon	ρ_{carbon}	g cm^{-3}	2.26
Density of PTFE	ρ_{PTFE}	g cm^{-3}	2.16
Density of electrolyte	$\rho_{electrolyte}$	g cm^{-3}	1.04
Density of aluminum		g cm^{-3}	2.7
Density of stainless steel		g cm^{-3}	7.4–8.0

The total ($M_{\text{Li tot cell}}$) and theoretical ($M_{\text{Li th cell}}$) masses of lithium in an individual cell are

$$M_{\text{Li tot cell}} = \frac{M_{\text{Li tot}}}{N_{\text{cells}}} \tag{6}$$

$$M_{\text{Li th cell}} = \frac{M_{\text{Li th}}}{N_{\text{cells}}} \tag{7}$$

The total mass of lithium in a cell is used in calculating the cell mass and volume; the theoretical mass of lithium in a cell is used in calculating the mass and volume of discharge products and the specific and volumetric cell capacities.

The volume of lithium in the cell ($V_{\text{Li cell}}$) is given by

$$V_{\text{Li cell}} = \frac{M_{\text{Li tot cell}}}{\rho_{\text{Li}}} \tag{8}$$

The cathode is assumed to consist of only carbon and polytetrafluoroethylene (PTFE). The mass of the cathode (M_{cathode}) is dependent on the percentage of carbon in the cathode and the cathode capacity per mass of carbon.

$$M_{\text{cathode}} = \frac{M_{\text{Li th cell}} \times F \times 1000}{n \times MW_{\text{Li}} \times C_{\text{cathode}} \times x \times 3600} \tag{9}$$

where C_{cathode} is the cathode capacity in units of mAh g^{-1} carbon and x is the percent carbon in the cathode. It is assumed that 100% of the active material in the cathode is utilized.

The mass of electrolyte ($M_{\text{electrolyte}}$) is based on the mass of the cathode. In commercial lithium-ion batteries, the electrolyte mass is approximately 15% of the cathode mass [15]. This percentage was used in this analysis to estimate the mass of the electrolyte

$$M_{\text{electrolyte}} = M_{\text{cathode}} \times 0.15 \tag{10}$$

The volume of the cathode is dependent on the volume of the discharge product, the volume of electrolyte, and any additional pore volume necessary for gas transport. The discharge product is assumed to be 100% Li_2O_2.

The mass of lithium peroxide ($M_{Li_2O_2}$) is calculated for 100% depth of discharge (DOD) based on the theoretical amount of lithium in a cell, since this represents the mass of lithium upon which the energy of the pack is based. The overall reaction is

$$2Li + O_2 \leftrightarrow Li_2O_2 \tag{11}$$

and the discharge product mass is

$$M_{Li_2O_2} = \frac{M_{\text{Li th cell}} \times MW_{Li_2O_2}}{2 \times MW_{\text{Li}}} \tag{12}$$

where $MW_{Li_2O_2}$ is the molecular weight for lithium peroxide.

The volume of discharge product ($V_{Li_2O_2}$) is then

$$V_{Li_2O_2} = \frac{M_{Li_2O_2}}{\rho_{Li_2O_2}} \tag{13}$$

where $\rho_{Li_2O_2}$ is the density of Li_2O_2.

The volume of electrolyte ($V_{\text{electrolyte}}$) is calculated as

$$V_{\text{electrolyte}} = \frac{M_{\text{electrolyte}}}{\rho_{\text{electrolyte}}} \tag{14}$$

where $\rho_{\text{electrolyte}}$ is the density of the electrolyte.

The minimum pore volume in the cathode ($V_{\text{min pore}}$) is the sum of the discharge product volume and the electrolyte volume

$$V_{\text{min pore}} = V_{Li_2O_2} + V_{\text{electrolyte}} \tag{15}$$

i.e., the discharge product completely fills the empty pore volume of the cathode at the end of discharge. Since this leaves no available pore volume for gas transport, the total pore volume in the cathode ($V_{\text{tot pore}}$) must be greater than the minimum amount.

$$V_{\text{tot pore}} = V_{\text{min pore}} \times V_{\text{ex pore}} \tag{16}$$

where $V_{\text{ex pore}}$ is the excess pore volume multiplier in the cathode and has values of ≥ 1.

The total volume of the cathode is the sum of the total pore volume and the cathode material volumes ($V_{\text{cath mat}}$) for carbon and PTFE

$$V_{\text{cath mat}} = M_{\text{cathode}} \left(\frac{x}{\rho_{\text{carbon}}} + \frac{(1-x)}{\rho_{\text{PTFE}}} \right) \tag{17}$$

where ρ_{carbon} and ρ_{PTFE} are the densities of carbon and PTFE, respectively, and x is the mass fraction of carbon in the cathode.

The total volume of the cathode ($V_{\text{tot cath}}$) is then given by

$$V_{\text{tot cath}} = V_{\text{tot pore}} + V_{\text{cath mat}} \tag{18}$$

The porosity of the cathode (ε) can then be calculated by

$$\varepsilon = \frac{V_{\text{tot pore}}}{V_{\text{tot cath}}} \tag{19}$$

The volume (V_{sep}) and mass (M_{sep}) of the separator are

$$V_{\text{sep}} = z_{\text{sep}} \times A_{\text{plate}} \tag{20}$$

$$M_{\text{sep}} = \frac{V_{\text{sep}}}{\rho_{\text{sep}}} \tag{21}$$

where z_{sep} and ρ_{sep} are the thickness and density of the separator, respectively.

The mass and volume of the bipolar plate are calculated as follows. The volume of the plate (V_{plate}) is equal to

$$V_{\text{plate}} = z_{\text{st plate}} \times A_{\text{plate}} \tag{22}$$

where $z_{\text{st plate}}$ is the thickness of the stamped plate. The thickness of the stamped plate is the sum of the unstamped plate thickness ($z_{\text{unst plate}}$) and the flow field depth ($z_{\text{flow field}}$).

$$z_{\text{st plate}} = z_{\text{unst plate}} + z_{\text{flow field}} \tag{23}$$

The mass of the plate (M_{plate}) is equal to

$$M_{\text{plate}} = \frac{V_{\text{unst plate}}}{\rho_{\text{plate}}} \tag{24}$$

where $V_{\text{unst plate}}$ is the unstamped plate volume and ρ_{plate} is the density of the plate material. The unstamped plate volume is given by

$$V_{\text{unst plate}} = z_{\text{unst plate}} \times A_{\text{plate}} \tag{25}$$

The total mass (M_{cell}) and volume (V_{cell}) of the cell components are then given by

$$M_{\text{cell}} = M_{\text{Li tot cell}} + M_{\text{cathode}} + M_{\text{electrolyte}} + M_{\text{sep}} + M_{\text{plate}} \tag{26}$$

$$V_{\text{cell}} = V_{\text{Li cell}} + V_{\text{cathode}} + V_{\text{electrolyte}} + V_{\text{sep}} + V_{\text{plate}} \tag{27}$$

Note that the electrolyte volume is not explicitly included in the calculation of the cell volume because it is already included in the cathode volume.

The specific and volumetric cell capacities ($C_{\text{sp cell}}$ and $C_{\text{vol cell}}$, respectively) are estimated by dividing the charge in the cell by the mass or volume of the cell.

$$C_{\text{sp cell}} = \frac{M_{\text{Li th cell}} \times F}{MW_{\text{Li}} \times M_{\text{cell}} \times 3600} \tag{28}$$

$$C_{\text{vol cell}} = \frac{M_{\text{Li th cell}} \times F}{MW_{\text{Li}} \times V_{\text{cell}} \times 3600} \tag{29}$$

The specific and volumetric energy densities (E_{sp} and E_{vol}, respectively) are calculated as

$$E_{\text{sp}} = C_{\text{sp cell}} \times CV_{\text{disch}} \tag{30}$$

$$E_{\text{vol}} = C_{\text{vol cell}} \times CV_{\text{disch}} \tag{31}$$

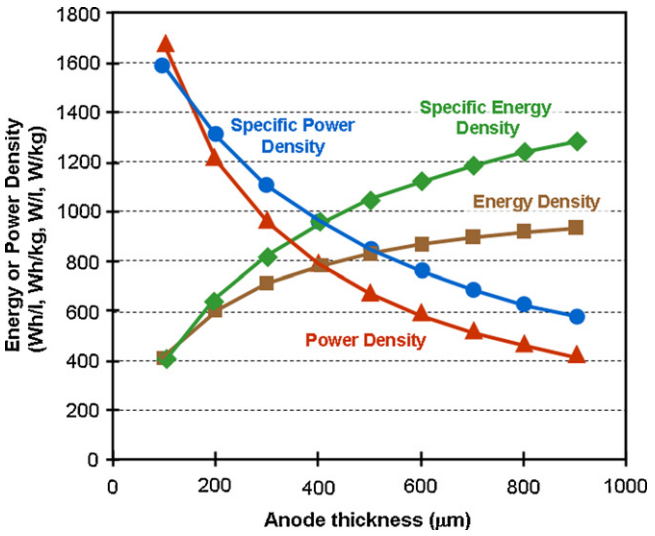

Fig. 2. Effect of Li anode thickness on energy and power density. Squares and triangles are volumetric energy and power density, respectively; diamonds and circles are specific energy and power density, respectively.

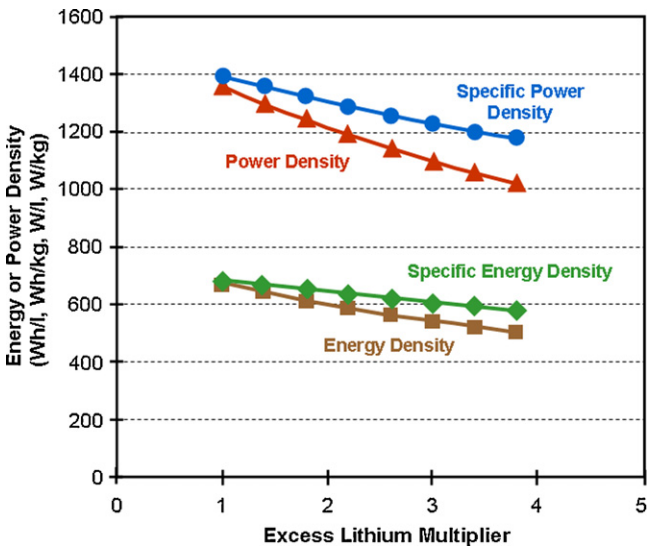

Fig. 3. Effect of excess lithium on energy and power density. Squares and triangles are volumetric energy and power density, respectively; diamonds and circles are specific energy and power density, respectively.

The cell current (I_{cell}) is given by

$$I_{cell} = \frac{i \times A_{plate}}{1000} \tag{32}$$

where i is the current density in mA cm^{-2}, and the 1000 converts mA to A. The cell power (P_{cell}) is calculated as

$$P_{cell} = I_{cell} \times CV_{disch} \tag{37}$$

The specific and volumetric power densities (P_{sp} and P_{vol}, respectively) are given by

$$P_{sp} = \frac{P_{cell}}{M_{cell}} \tag{38}$$

$$P_{vol} = \frac{P_{cell}}{V_{cell}} \tag{39}$$

3. Results

The cell performance targets, the SOA lithium-air cell performance values, and the bipolar plate cell performance estimates are shown in Table 3. Using parameters from Table 1, it has been shown that the energy and power density targets can be achieved with a bipolar plate design. The influence of individual parameters on cell performance and the rational for selecting the values in Table 1 is described below.

3.1. Lithium anode thickness

The effect of the Li anode thickness on the energy and power densities is shown in Fig. 2, using a constant plate area of 500 cm^2. As the anode thickness increases, the energy densities increase while the power densities decrease. The energy densities increase because the increase in the mass of lithium per cell ($M_{Li\ tot\ cell}$) more than offsets the increase in cell mass and volume. In contrast, the power densities decrease strictly due to the increase in cell mass and volume. Thus, to meet the energy and power density targets of 600 Wh l^{-1} and 1200 W l^{-1}, respectively, the anode thickness must be ≤200 μm. In this study, the anode thickness is set equal to 200 μm.

3.2. Excess lithium

During the course of battery cycling, electrochemically active lithium is lost at both the anode and cathode. On the anode side, growth of inactive moss and dendrites contributes to lithium loss. At the cathode, unreacted discharge products from incomplete recharge contribute to lithium loss. An excess lithium multiplier (Li_{ex}) of 1 corresponds to the minimum amount of lithium needed to meet the energy requirements of the pack. In the literature, a Li_{ex} value of 4 has been discussed as necessary to meet cycle life requirements, which represents a 300% excess [16].

For a given plate area and number of cells, increasing the excess lithium results in a decrease in both the energy and power densities due to an increase in cell mass and volume, as shown in Fig. 3. In order to meet the energy density target of 600 Wh l^{-1}, the excess lithium multiplier must be ≤2.0; a value of 2.0 is used in this study. The allowable excess lithium which meets the energy density target is found to increase as the cathode capacity increases, as shown in Fig. 4. However, even at an extremely high capacity of 5000 mAh g^{-1} carbon, the excess lithium multiplier is still approximately 2.8. Minimizing the excess lithium in the cell will be particularly important in achieving the performance and cost targets, as discussed below.

3.3. Current density

Increasing the current density linearly increases the power densities, as shown in Fig. 5. As expected, the energy densities are independent of the value of the current density. To meet the power density target of 1200 W l^{-1}, the current density must be >42 mA cm^{-2}. Increasing the current density by over an order of magnitude from today's state-of-the-art values of 1.0 mA cm^{-2} represents a major technical challenge for successful development of lithium-air batteries for automotive applications. Note that at the SOA current density of 1 mA cm^{-2}, the maximum achievable power density is estimated to be only 29 W l^{-1}.

3.4. Cathode capacity

Increasing the cathode capacity increases both the energy and power densities, as shown in Fig. 6, due to decreases in the mass and volume of the cathode. However, cathode capacities above 2000 mAh g^{-1} carbon produce only modest gains in the energy and

Table 3
Comparison of technical targets to SOA and bipolar plate cell design.

	Cell target	SOA performance	Bipolar plate design
Specific energy density[a]	400 Wh kg^{-1}	250–350 Wh kg^{-1} [d] 48 Wh kg^{-1} [c]	640 Wh kg^{-1}
Volumetric energy density[a]	600 Wh l^{-1}	66 Wh l^{-1} [c]	600 Wh l^{-1}
Specific power density[b]	800 W kg^{-1}	0.8 Wh kg^{-1} [c]	1310 W kg^{-1}
Volumetric power density[b]	1200 W l^{-1}	1.0 Wh l^{-1} [c]	1220 W l^{-1}
System cost estimate	<$100 kWh^{-1}	–	$238 kWh^{-1}

[a] At C/3 discharge rate.
[b] 80% depth of discharge, 30 s.
[c] Estimated using electrode and membrane data from Ref. [12].
[d] From Ref. [1].

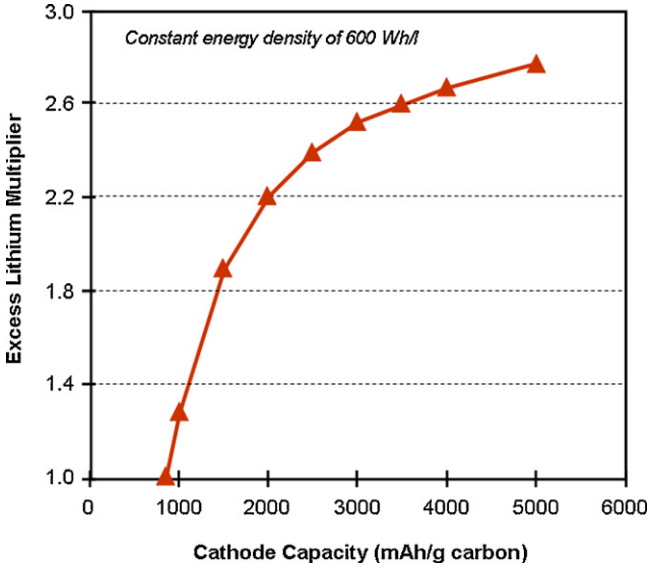

Fig. 4. Effect of cathode capacity on allowable excess lithium.

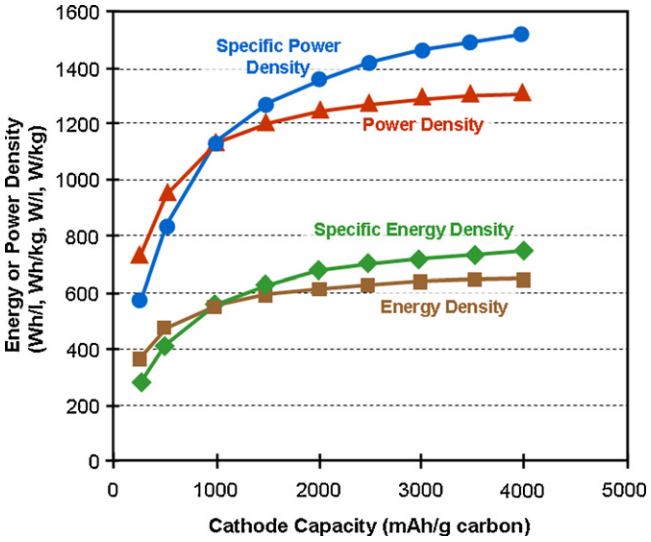

Fig. 6. Effect of cathode capacity on energy and power densities. Squares and triangles are volumetric energy and power density, respectively; diamonds and circles are specific energy and power density, respectively.

power densities. To meet the energy and power density targets of 600 Wh l^{-1} and 1200 W l^{-1}, respectively, a minimum cathode capacity of 1650 mAh g^{-1} carbon is needed. Note that 100% utilization of the cathode carbon is assumed in these calculations.

Fig. 7 shows the effect of cathode capacity on the cathode thickness at a constant energy density of 600 Wh l^{-1}. Thinner cathodes are desirable in order to improve mass transfer performance, but they require very high cathode capacities. Using a cathode capacity of 1650 mAh g^{-1} carbon results in a cathode thickness of approximately 300 μm, which is close to the thickness of cathode gas diffusion layers in PEM fuel cells.

The effect of cathode capacity and plate area on the cell energy density is shown in Fig. 8, where the number of cells was held

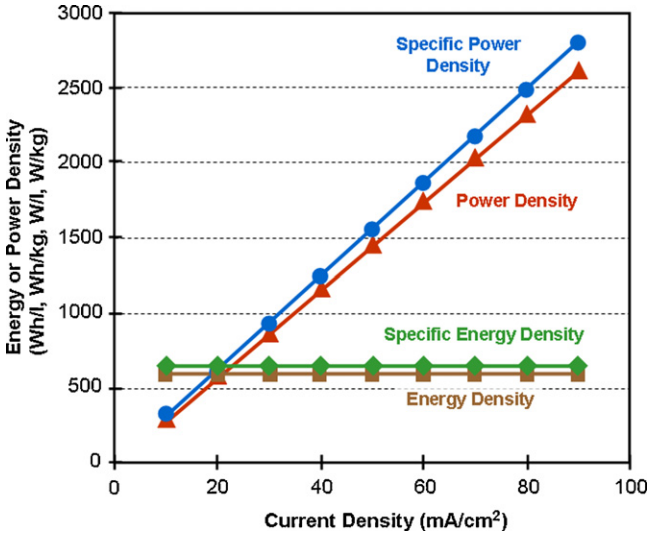

Fig. 5. Effect of current density on energy and power densities. Squares and triangles are volumetric energy and power density, respectively; diamonds and circles are specific energy and power density, respectively.

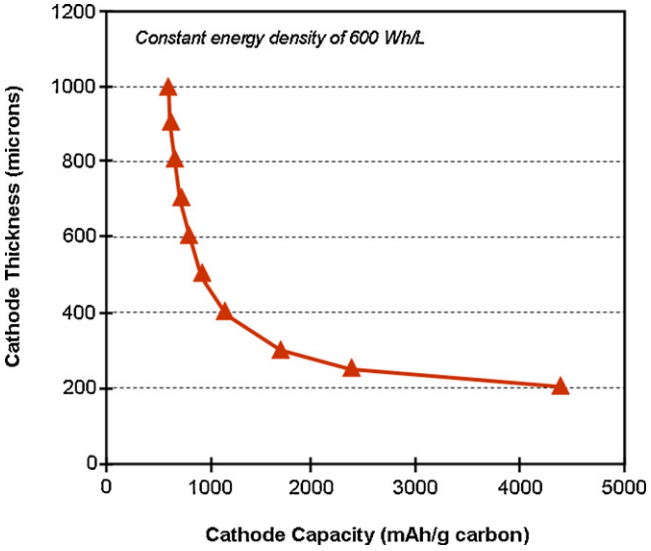

Fig. 7. Effect of cathode capacity on cathode thickness.

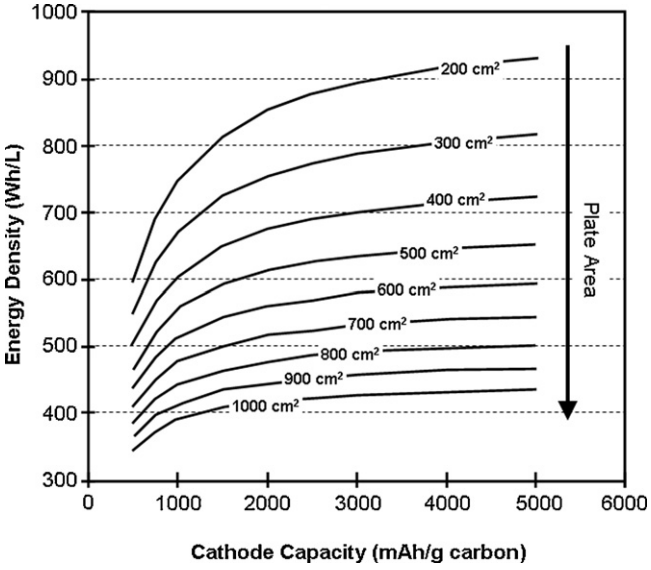

Fig. 8. Effect of cathode capacity and plate area on energy density.

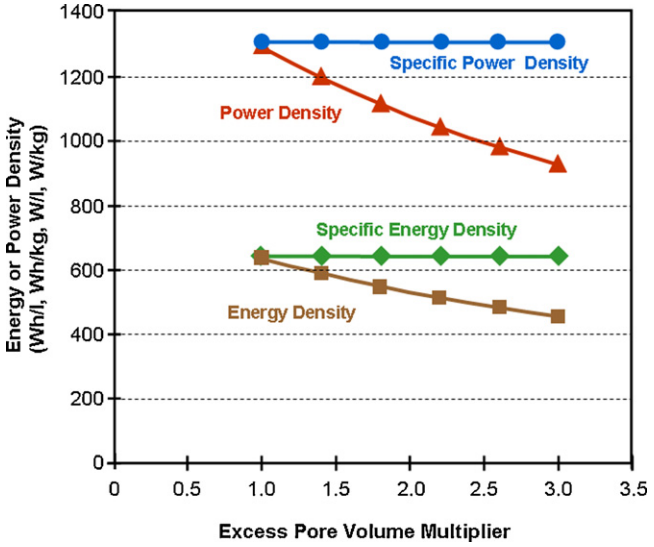

Fig. 9. Effect of excess pore volume on energy and power densities. Squares and triangles are volumetric energy and power density, respectively; diamonds and circles are specific energy and power density, respectively.

constant at 1434. As the plate area is increased, the energy density decreases for a given cathode capacity due to the increased cell mass and volume. With a plate area of 600 cm^2, the energy density target is not met, even at extremely large cathode capacities. In this study, a plate area of 500 cm^2 is chosen to meet the energy density target at a reasonable capacity. Although plate areas below 500 cm^2 would allow even lower cathode capacities to meet the energy density target, the lower plate area would require an even higher current density to meet the power density target.

The cathode porosity is also found to increase with an increase in cathode capacity. It is found that as the capacity increases, the volume occupied by the carbon and binder decreases. However, the pore volume for the discharge product remains constant for a given pack energy. Therefore, the pore volume to cathode volume ratio increases with increasing capacity, resulting in an increase in the porosity. Higher porosity cathodes could potentially support higher current densities due to improved gas transport. This suggests that higher cathode capacities could be useful in improving power densities beyond that estimated by these analyses.

3.5. Excess pore volume

As shown in Fig. 9, the energy and power densities decrease as the excess pore volume increases. As expected, the specific energy and specific power densities are independent of the value of the excess pore volume. The cathode structure must simultaneously minimize pore volume to maximize the energy and power densities while maximizing mass transfer to achieve high current densities. To meet the energy and power density targets, the excess pore volume multiplier must be $\leq$1.3; a value of 1.3 is used in this study, which set an upper limit on the cathode porosity of approximately 0.7. If an upper limit on the cathode porosity exists, the necessary current density and cathode capacity values estimated in this analysis would need to be increased.

3.6. Bipolar plate thickness, material density, and flow field depth

Metallic bipolar plates are produced by stamping the flow field into a metal plate. The plate material and the flow field depth determine the plate thickness necessary for successful stamping. As the plate thickness increases, the energy and power densities decrease due to increases in the cell mass and volume. In this study, the plate thickness is set to 200 μm, which corresponds to state-of-the-art fuel cell bipolar plates made from stainless steel. No attempt is made to determine the optimum manufacturing thickness for other materials such as aluminum.

The density of the plate material affects the specific energy and power densities, as shown in Fig. 10. The energy and power densities are independent of the plate material density since increasing the plate material density increases the cell mass, but not the cell volume. The material density must be less than 5 g cm^{-3} to meet the specific energy and specific power density targets of 400 Wh kg^{-1} and 800 W kg^{-1}, respectively. Stainless steel, which has a density of 7.4–8.0 g cm^{-3}, is not a viable material option for bipolar plates in a lithium-air battery; using stainless steel, the specific energy density target of 400 Wh kg^{-1} cannot be achieved, even with a cathode capacity of 5000 mAh g^{-1} carbon. In this study, the plate material is assumed to be aluminum, with a density of 2.7 g cm^{-3}.

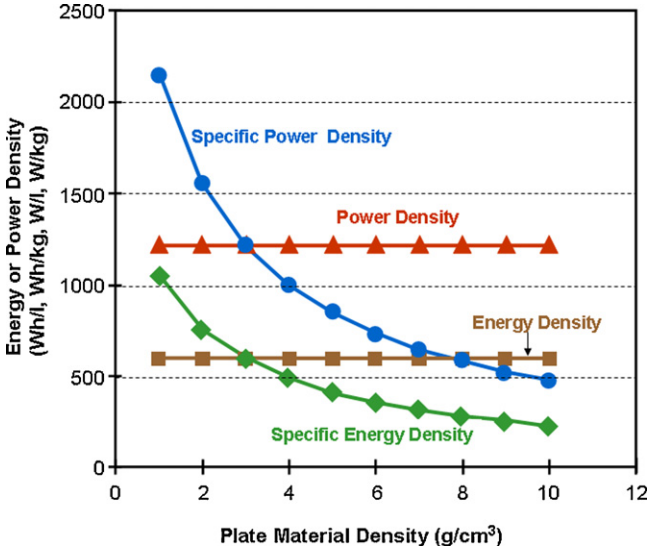

Fig. 10. Effect of plate material density on energy and power densities. Squares and triangles are volumetric energy and power density, respectively; diamonds and circles are specific energy and power density, respectively.

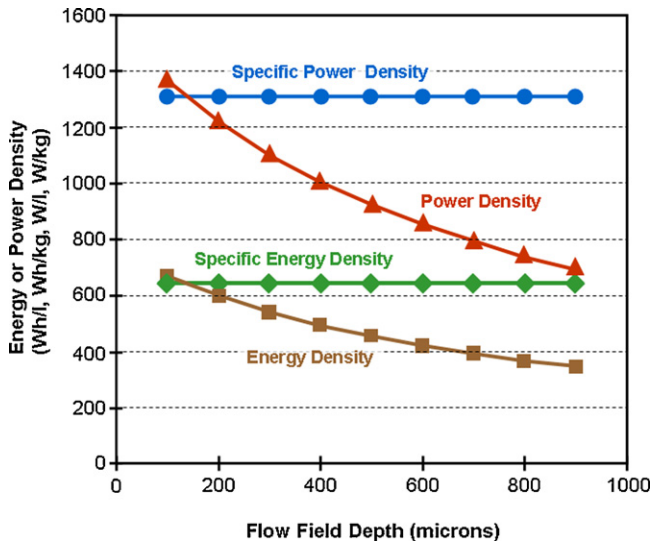

Fig. 11. Effect of flow field depth on energy and power densities. Squares and triangles are volumetric energy and power density, respectively; diamonds and circles are specific energy and power density, respectively.

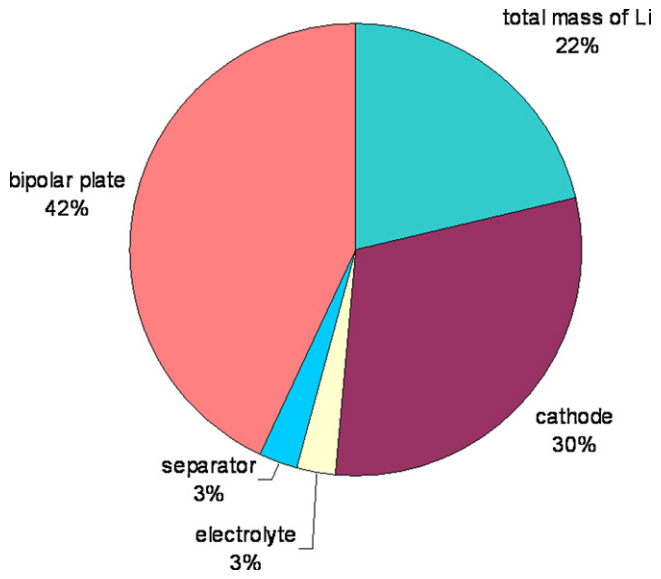

Fig. 13. Percent distribution of volume among cell components.

The flow field depth is determined by the air flow requirements at the cathode. The larger the flow field depth, the lower the parasitic power necessary for pumping air. However, increasing the flow field depth reduces the energy and power densities due to an increase in cell volume, as shown in Fig. 11. As expected, the specific energy and specific power densities are independent of flow field depth. To meet the energy density targets, the flow field depth must be ≤200 μm. In this study, the flow field depth is set equal to 200 μm, which represents state-of-the-art design for PEM fuel cells. Because water management is not an issue for lithium-air batteries, the flow field depth could potentially be reduced.

3.7. Cell mass, volume, and capacity

The percent distributions of mass and volume among the cell components are shown in Figs. 12 and 13, respectively. The bipolar plate is the major cell component in terms of both mass and volume followed by the cathode; together, these two components account for over 80% of the cell mass and 70% of the cell volume. Although no catalyst is included in these distributions, the catalyst is estimated to account for less than 5% of the cell mass and volume based on published data [7,17].

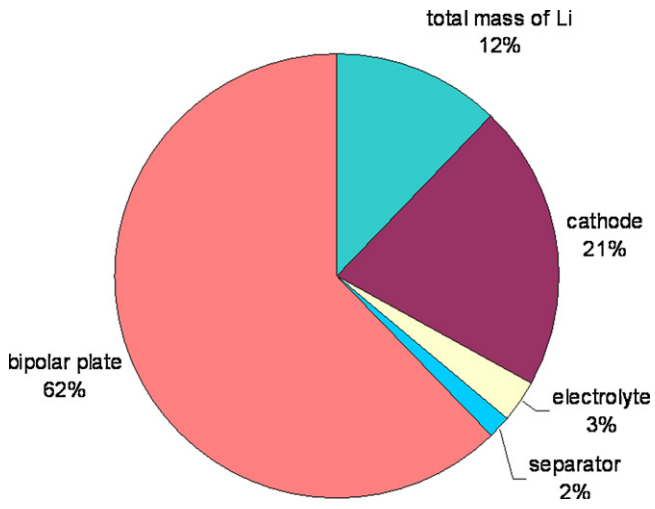

Fig. 12. Percent distribution of mass among cell components.

In the literature, capacities are routinely reported per mass of carbon or per mass of active material in the cathode, ignoring the other cell components. For automotive applications, however, the most useful metrics are per mass or volume of the cell. The total cell mass and volume are estimated at 43.4 g and 46.5 cm^3, respectively, with corresponding cell capacities of 238 mAh g^{-1} cell and 222 mAh cm^{-3} cell.

3.8. Cost analysis

The lithium-air system cost estimate is based on an advanced, high-volume manufacturing cost estimate of \$49 kW_{net}^{-1} for a fully assembled, 80 kW_{net} PEM fuel cell system [18]. The fuel cell system consists of a fuel cell stack constructed of stamped stainless steel bipolar plates and the balance-of-plant (BOP) components for fuel and air subsystems, thermal management, and controls.

The fuel cell stack component costs and the estimated lithium-air pack costs are shown in Table 4. Modifications to the fuel cell component costs include removing Pt catalyst and ink costs, deleting costs for the anode plate and GDL, reducing the membrane cost to reflect the lower cost of a polypropylene battery separator compared to Nafion (\$4.50 m^{-2} vs. \$25 m^{-2}, respectively), using aluminum instead of 316 SS for the plate material, and adding the material cost of the lithium metal anode (\$110 kg^{-1}) with an excess lithium multiplier of two. The total pack cost is then adjusted to account for the differences in the cell active area and the number of cells between the fuel cell stack and the lithium-air pack (339 cm^2 vs. 500 cm^2 per cell and 372 vs. 1434 cells, respectively). This results in a lithium-air pack cost of \$8030. The fuel cell BOP costs and the estimated lithium-air BOP costs are shown in Table 5. Modifications to the BOP costs for the lithium-air system involve removing the cost for the fuel loop. This results in a lithium-air BOP cost of \$1475. The total 40 kWh lithium-air system cost is then estimated at \$9500, or \$238 kWh^{-1}. This exceeds the system cost goal of \$100 kWh^{-1}.

Opportunities for cost reduction may exist in both the pack and BOP costs, with the focus on the components or subsystems with the highest percentage cost. For the pack, the lithium anode represents over 50% of this cost; the next largest component is the frame/gasket for the separator/cathode assembly at approximately

Table 4
Component costs for PEM fuel cell stack and lithium-air battery pack.

Components	PEM FC stack	Li-air pack	Notes
Bipolar plates	$195.52	$19.64	Only cathode plate used; Al instead of SS
MEAs			For Li-air, membrane/cathode assembly
Membranes	$104.83	$18.87	Nafion – $25 m^{-2}; PP or PE – $6 m^{-2}
Catalyst ink & application	$356.89	0	No Pt
GDLs	$114.88	$57.44	Only cathode GDL used
M&E hot pressing	$7.55	$7.55	
M&E cutting & slitting	$2.76	$2.76	
MEA frame/gasket	$156.98	$156.98	Frame/gasket for separator cathode
Coolant gaskets	$12.11	$12.11	
End gaskets	$0.30	$0.30	
End plates	$16.56	$16.56	
Current collectors	$4.35	$4.35	
Compression bands	$5.00	$5.00	
Stack assembly	$17.84	$17.84	
Stack conditioning	$6.27	$6.27	
Stack cost	$1001.84	$325.67	
Number of stacks	2	2	
		$651.34	Li pack cost without anode
Li metal cost		$760.36	Li metal anode cost; excess Li = 2
Total stack cost	$2003.68	$1411.69	
Cost per active area per cell	$0.0159	$0.0112	Based on 339 cm^2 per cell and 372 cells
Total Li-air pack cost		$8030	Based on 500 cm^2 per cell and 1434 cells

20%. For the BOP, the air loop cost represents the largest single subsystem at approximately 35%.

The above analysis represents a reasonable cost estimate based on engineering judgment. However, accurate system costs cannot be calculated by merely subtracting or adding different components in the system. Significant design differences exist between a lithium-air system and PEM fuel cell system in terms of fuel, design and materials for the bipolar plates, electrode designs, and the air subsystem requirements. For an accurate cost estimate, the effects of design, materials, and scaling changes must be included.

4. Discussion

The calculations presented in this work are iterative and interrelated, and represent a snapshot of a potentially viable automotive lithium-air battery system using a bipolar plate cell design. Other cell designs will result in different critical parametric sets and values. The key findings of this design study are discussed below along with their implications in guiding future lithium-air battery research for automotive applications.

4.1. Current density

Perhaps the most challenging finding is the current density requirement of >40 mA cm^{-2}, which represents greater than an order of magnitude increase over SOA research cells. While considerable literature has been published on improving cathode capacity and cycle life, little effort has been focused on improving current density. The majority of results reported in the literature are obtained at current densities of 0.05–0.2 mA cm^{-2} using pure oxygen. In an automotive application, the low current density problem will be further compounded by the practical need to operate the battery on air, which has proven difficult in the literature. More experimental data are needed – operating at higher current densities with air – to assess the SOA performance of a lithium-air battery for automotive applications. Increased focus on current densities will be required to achieve the necessary increase; if not, the lithium-air battery will simply be too big to fit in the available space on the vehicle.

4.2. Cathode design

The cathode design for a lithium-air battery must simultaneously satisfy multiple requirements. The cathode must achieve a high capacity with high utilization in order to meet the energy density targets. The cathode structure must also support high oxygen mass transfer rates necessary for achieving high current densities. This same structure must also allow the homogeneous distribution and recycle of solid products during discharge and charge, respectively, while maintaining electrolyte and electronic conductivity. Designing a cathode that can satisfy the above, sometimes contradictory, requirements represents a significant technical challenge.

The minimum cathode capacity of 1650 mAh g^{-1} carbon identified in this study appears possible based on published results, but assumes 100% utilization of the electrode in a discharge/charge cycle. Because commercial secondary batteries utilize only a fraction of an electrode capacity in a typical cycle, the actual capacity required for the cathode could be 2–3 times greater than the minimum identified in this study. Alternatively, the cathode thickness could be increased to increase the cell capacity for a cycle. However, thicker cathodes will most likely reduce the mass transfer rates of oxygen and make it even more difficult to achieve the increase in current density required for meeting the power density target. While high specific capacity materials have been developed, the development of relatively thick cathodes (>300 μm) with high utilization remains an area unexplored in the literature, where thin films <100 μm are typically used.

4.3. Lithium anode

Changes in the anode surface can have a significant impact on the battery cost, since production of electrochemically inactive

Table 5
BOP costs for PEM fuel cell system and lithium-air battery system.

Components	PEM FC system	Li-air system
Mounting frames	$30.00	$30.00
air loop	$553.20	$553.20
Coolant loop	$275.55	$275.55
Fuel loop	$457.20	$0
System controllers/sensors	$200.00	$200.00
Miscellaneous	$415.78	$415.78
Total BOP cost	$1931.73	$1474.53

lithium over the lifetime of the battery requires a large excess of lithium in the anode to meet cycle life and capacity targets. Also, shorting due to dendritic growth has obvious safety implications that must be managed. The application of pressure between the separator and the lithium metal anode can inhibit dendritic formation, produce densely packed deposits, and prevent electrical isolation of individual dendrites/particles during charge/discharge, resulting in high cycling efficiency [19–22]. In a bipolar plate design, the pressure between cell components is easily controlled, which may help reduce the amount of excess lithium required to meet the performance targets and minimize cost.

The dimensional changes that occur at a planar anode during charge and discharge must be minimized in order to maintain electrical contact and seal integrity. For example, an anode with an excess lithium of 2 will experience a 50% decrease in thickness at full discharge, i.e., an initial anode thickness of 200 μm will decrease to 100 μm at full discharge. If a battery module consisted of 100 cells with the above anode, the total dimensional change in the module would be 1 cm. At this time, the magnitude of dimensional changes that can be tolerated at the electrodes in the bipolar plate cell design is unknown. It is possible that alternatives to strictly planar anodes will be necessary to provide sufficient surface area and minimize dimensional changes.

5. Conclusion

A bipolar plate cell design for a lithium-air battery can meet the cell performance targets, but not the system cost target derived from the USABC system goals for EVs. In addition, preliminary design targets for cell parameters have been established in order to meet these performance targets. In particular, the excess lithium multiplier should be $\leq$2.0, the current density should be >40 mA cm^{-2}, the cathode capacity should be >1650 mAh g^{-1} carbon, and the bipolar plate material density should be <5 g cm^{-3}.

The bipolar plate design represents the most successful cell design used for PEM fuel cells and has been used in other batteries. For lithium air batteries, however, this design imposes an additional mass and volume penalty necessary for moving air through the cell that is not required in other batteries. Because the bipolar plate accounts for over 60% and 40% of the cell mass and volume, respectively, the performance of the cell is highly sensitive to the plate thickness, material density, and the flow field depth. Because of this sensitivity, the design will require further research to improve performance and meet the system cost targets.

References

[1] K.M. Abraham, Z. Jiang, J. Electrochem. Soc. 143 (1996) 1.
[2] J. Read, J. Electrochem. Soc. 149 (2002) A1190–A1195.
[3] S. Zhang, D. Foster, J. Read, J. Power Sources 195 (2010) 1235–1240.
[4] A. Dobley, C. Morein, K.M. Abraham, 208th ECS Meeting, #323, 2005.
[5] J. Zheng, D. Wang, W. Xu, J. Xiao, R.E. Williford, J. Power Sources 195 (2010) 4332–4337.
[6] T. Ogasawara, A. Debart, M. Holzapfel, P. Novak, P. Bruce, J. Am. Chem. Soc. 128 (2006) 1390–1393.
[7] A. Debart, J. Bao, G. Armstrong, P. Bruce, J. Power Sources 174 (2007) 1177–1182.
[8] J. Read, J. Electrochem. Soc. 150 (2003) A1351–A1356.
[9] J. Zheng, R. Liang, M. Hendrickson, E. Plichta, J. Electrochem. Soc. 155 (2008) A432–A437.
[10] F. Wagner, B. Lakshmanan, M. Mathias, J. Phys. Chem. Lett. 1 (2010) 2204–2219.
[11] A. Dobley, C. Morein, R. Roark, ECS Trans. 3 (2008) 83–88.
[12] S. Beattie, D. Manolescu, S. Blair, J. Electrochem. Soc. 156 (2009) A44–A47.
[13] H. Cheng, K. Scott, J. Power Sources 195 (2010) 1370–1374.
[14] USABC, Goals for Advanced Batteries for EVs, Energy Storage System Goals, http://www.uscar.org/guest/teams/12/U-S-Advanced-Battery-Consortium (October 14, 2010).
[15] D. Linden, T. Reddy, Handbook of Batteries, 3rd ed., McGraw-Hill, New York, 2002.
[16] J. Dahn, Presentation at the Almaden Institute, San Jose, CA, August 26–27, 2009.
[17] Y. Lu, H. Gasteiger, M. Parent, V. Chiloyan, Y. Shao-Horn, Electrochem. Solid-State Lett. 13 (2010) A69–A72.
[18] B. James, J. Kalinoski, Mass production cost estimation of automotive fuel cell systems, in: DOE H_2 Program Review, May 21, 2009, Directed Technologies, Inc., 2009.
[19] L. Gireaud, S. Grugeon, S. Laruelle, B. Yrieix, J. Tarascon, Electrochem. Commun. 8 (2006) 1639–1649.
[20] T. Hirai, I. Yoshimatsu, J. Yamaki, J. Electrochem. Soc. 141 (1994) 611–614.
[21] D. Wilkinson, D. Wainwright, J. Electroanal. Chem. 355 (1993) 193.
[22] Z. Takehara, J Power Sources 68 (1997) 82–86.